Solidelectrolyte interphase evolution of carbon-coated silicon nanoparticles for lithium-ion batteries monitored by transmission electron microscopy and impedance spectroscopy

Reference:

Van Havenbergh Kristof, Turner Stuart, Driesen Kris, Bridel Jean-Sébastien, van Tendeloo Gustaaf.- Solidelectrolyte interphase evolution of carbon-coated silicon nanoparticles for lithium-ion batteries monitored by transmission electron microscopy and impedance spectroscopy

Energy Technology - ISSN 2194-4288 - 3:7(2015), p. 599-708

DOI: http://dx.doi.org/doi:10.1002/ente.201500034

SEI-Evolution of Carbon-Coated Si Nanoparticles monitored by Transmission Electron Microscopy and Impedance Spectroscopy

Kristof Van Havenbergh, Stuart Turner, Kris Driesen, Jean-Sébastien Bridel and Gustaaf Van Tendeloo*

K. Van Havenbergh, Dr. S. Turner, Prof. Dr. G. Van Tendeloo
EMAT, University of Antwerp, Groenenborgerlaan 171, B-2020 Antwerp, Belgium

K. Van Havenbergh, Dr. K. Driesen, Dr. J.-S. Bridel
Umicore Research, Watertorenstraat 33, B-2250 Olen, Belgium
E-mail: Jean-Sebastien.Bridel@eu.umicore.com

Keywords: Li-ion batteries, coated silicon nanoparticles, SEI, impedance spectroscopy, TEM

Abstract:

The main drawbacks of silicon as the most promising anode material for Li-ion batteries (3572 $mAh.g^{-1}$) are lithiation-induced volume changes and the continuous formation of a Solid Electrolyte Interphase (SEI) upon cycling. A recent strategy is to focus on the influence of coatings and composite materials. To this end, the evolution of the SEI, as well as an applied carbon coating, on nanosilicon electrodes during the first electrochemical cycles is monitored. Two specific techniques are combined: Transmission Electron Microscopy (TEM) is used to study the surface evolution of the nanoparticles on a very local scale, whereas Electrochemical Impedance Spectroscopy (EIS) provides information on the electrode level. A TEM-EELS fingerprint signal of carbonate structures from the SEI is discovered, which can be used to differentiate between SEI and a graphitic carbon matrix. Furthermore, the shielding effect of the carbon coating and the thickness evolution of the SEI is described.

1. Introduction

Scientists agree that the 21st century will be defined by an energy transition, in which hydrocarbons will be replaced as the privileged global fuel by sustainable energy sources. To fulfill the ever-increasing demand for portable electrical energy, e.g. electrical vehicles and portable electronics, there will be a need for an efficient and reliable storage mechanism.[1]

Lithium ion batteries are the most suitable candidates for these applications, due to their high volumetric and gravimetric energy density, reliability and energy efficiency.[2, 3] Many small improvements have been achieved on the level of high energy cathode materials.[4] However, a significant improvement of total battery capacity can only be achieved if the anode capacity is improved correspondingly. Since the commercialization of the first Li-ion battery by the Sony corporation in 1990 with graphite as anode active material, researchers have been searching for an alternative to graphite in order to meet the high energy capacity demands of today.[5]

The possibility of an electrochemical Li-alloying reaction with semi metals such as Si, Sn, etc. with a high theoretical capacity was proven in the 1970's and was shown to be highly promising.[6] Silicon is the best candidate with a theoretical capacity of 3579 $mAh.g^{-1}$ (10-fold higher theoretical capacity than graphite: 372 $mAh.g^{-1}$). However, commercial uses have been limited because of two major issues concerning the use of silicon as an anode material. The first is the large volume changes (~275%) that are associated with the (de)alloying reaction of silicon with lithium,[3, 5-7, 8] causing pulverization of the silicon particles and disintegration of the electrode.[9, 10] The second is the formation of the so-called Solid Electrolyte Interphase (SEI) on silicon surfaces, due to reaction with the electrolyte, which also cannot support the huge volume expansion.[11] New silicon surfaces are exposed every electrochemical cycle, causing continuous SEI-formation, consumption of active lithium and consequently capacity loss.[12] To overcome these issues, one approach is to change the morphology of the anode material to avoid the problems with the volume variation.[13] The use of nanowires has been described,[3, 14] where the volume increase is limited to only one direction (longitudinal direction of the nanowires). In addition, it was demonstrated that the integrity of nanoparticles with a small diameter can also be maintained.[15] Indeed, large particles have the tendency to fracture upon cycling, whereas this has not been observed for particles with a diameter smaller than 150 nm.[10] Besides the morphology, researchers also investigate the possibility

of SiO_x as an anode material. An outstanding cycling durability with a reversible capacity of 1000 $mAh.g^{-1}$ after 2000 cycles was achieved by electrodeposition of SiO_x on a copper substrate, due to the suppression of crack formation in this matrix.[16] Another approach is the use of carboxymethyl cellulose (CMC), poly(acrylic acid) (PAA), poly(vinyl alcohol) (PVA) or alginate instead of poly(vinylidene fluoride) (PVDF) as an electrode binder.[17] They favor a better bonding between Si nanoparticles, resulting in a better electrode unity and capacity retention.[5, 18] The last major strategy is to act on the electrolyte and thus indirectly on the nature of the SEI. Electrolyte additives such as fluoroethylene carbonate (FEC) and vinylene carbonate (VC) can tune the SEI-stability and under specific conditions, the electrochemical performances of Si-based anodes were drastically improved.[19, 20]

Today, the main effort for commercialization is oriented on the use of coatings and composites in order to solve the problems due to volume expansion.[21, 22-25] This strategy is known to improve the conductivity of the electrode while retaining the capacity. However, many parameters like the impact of a coating on the silicon anode material and on the SEI-formation are still unknown and are of crucial importance for further development (improvement).

In order to use these materials on an industrial scale, the interface between a coating or composite matrix and silicon has to be completely understood, taking particular interest in the influence on SEI formation and stability. Because the interface between silicon and the composite matrix is in the nanoscale region and is extremely sensitive, it is definitely not straightforward to investigate. A wide range of techniques has already been used, each one with its own advantages and disadvantages. Examples of techniques that are frequently used are: Scanning Electron Microscopy (SEM),[11, 23, 24] X-Ray Diffraction (XRD),[26, 27] X-ray Photoelectron Spectroscopy (XPS) [11, 12, 28, 29] and Infra-Red spectroscopy (IR).[11, 28] The main drawback of the mentioned techniques is that they are active on the electrode-level and less suitable for the particle surface-level.

In this study, two dedicated techniques, Transmission Electron Microscopy (TEM) and Electrochemical Impedance Spectroscopy (EIS), were used to investigate the impact of a carbon coating on silicon during electrochemical cycling. Advanced TEM is a technique that can give a unique insight into the mechanisms that are of importance at the electrode interface, at nanoscale and even atomic resolution. EIS on the other hand is a powerful analysis tool to study the different aspects of electrode kinetics, interfacial changes and the formation of SEI.[22-26, 30, 31] The combination of both techniques gives us the opportunity to link information on the nanoscale (TEM) with more averaged data on the electrode scale (EIS). This in-depth study was performed on two silicon materials: a pristine silicon nanopowder (p-Si) as a reference together with a carbon-coated silicon powder (c-Si). Both silicon materials (coated and uncoated) were studied with TEM and EIS at different states of charge. Comparing both materials during electrochemical cycling will allow us to study the influence of a carbon coating on the behavior of the silicon materials. The system simplicity makes the materials ideal to study the processes that play at the electrode interface.

2. Results and discussion

2.1. Interface evolutions during the first two electrochemical cycles

2.1.1. Local study by TEM

The TEM images of the initial electrode materials p-Si (**Figure 1**a) and c-Si (Figure 1b) display the crystallinity of the materials. The specifications of the surface layers of the particles are provided in the experimental section below. Both silicon powders, p-Si and c-Si, were electrochemically cycled and stopped at four selected points (Figure 1c), namely at the end of lithiation and delithiation in the first two cycles, for a detailed TEM investigation. **Figure 2**a and b show a TEM image and an electron energy-loss spectroscopy (EELS) chemical map respectively of some p-Si particles in fully lithiated state (0 V) in the first cycle. The chemical maps were generated using the program EELSModel.[32] This approach can

provide insight into the bonding and/or valency of the probed elements through the fine structure of the acquired EELS edges. For example, the shape of the Si $L_{2,3}$ edge, allows to differentiate between Si^0 and Si^{4+}.[33] By fitting the Si $L_{2,3}$ edge with a reference for Si^0 and Si^{4+}, the distribution of both can be mapped out, like in Figure 2b. Compared to the initial material in Figure 1a, large surface modification has taken place. The lithiated silicon particles have become partly amorphous [34] and the oxide layer at the surface has become much thicker (average 16 ± 1 nm). A crystalline core remains, indicating an incomplete Li-insertion process. It is interesting to mention here that a polygonal shape of the crystalline silicon core, originating from the preferential lithiation of certain facets in crystalline silicon, can be observed.[8, 35] The chemical map shows the distribution of various elements present in the sample and indicates that the surface layer is composed of oxidized silicon products. This observation corresponds with reports in literature where the native oxide layer is converted in lithium silicates (Li_4SiO_4) due to reactions with the electrolyte and SiO_xF_y due to reaction with the lithium salt $LiPF_6$.[12, 28, 29, 36, 37] It is important to keep in mind that the acquisition of the EELS data involves an intense interaction of the electron beam with the electrode material under investigation. As a result, there is the possibility that some of the volatile components, especially in the SEI, are altered or evaporated during data acquisition. Although this makes the technique less suitable to study the exact composition of the SEI, it remains well-suited to visualize the chemical distribution at the surface of the electrode materials.

Figure 2c and d show TEM images of the p-Si powder when cycled for one complete first cycle, from OCV to 0.01V and back until 1.5 V. The SEI layer at the surface of the particles was observed to be slightly thinner (14 ± 1 nm) but less stable under the electron beam as compared to the lithiated state. A similar phenomenon has been reported for graphite surfaces,[38] where a dynamic behavior of the SEI layer was observed, with thickening of the SEI at lower potentials and a thinning-out of the layer at 1.5 V. The distribution map in Figure 2d indicates that the surface of the particles is composed of oxidized silicon components.

Furthermore, a specific carbon signal can be observed at the extreme surface of the particles (see **Figure 3** and **Figure 4**). This signal originates from carbon-containing components of the SEI, such as Li_2CO_3 and/or lithium alkyl carbonates.[39, 40] It is described in literature that the outer part of the SEI layer is composed of organic components, whereas the inner part consists of inorganic species (silicates).[40] Note that part of the SEI can also be formed by the conductive agents present in the electrode, since they also participate in the lithiation reaction. During lithiation in the second cycle, the thickness of the SEI layer continued to increase (Figure 2e and f). The presence of the SEI layer makes the surface of the particles very rough. Furthermore, we managed to observe a trace of lithium at the surface, indicating that this SEI layer is composed of Li-containing structures. Si-Li alloy could not be observed, as lithium in this state evaporates immediately upon illumination by the electron beam. Furthermore, a carbonaceous SEI was also observed. Finally, the SEI layer again decreased in thickness in the delithiated state of the second electrochemical cycle (Figure 2g and h). Here, no lithium was detected at the surface. This is again in accordance with literature, where it is reported that some Li-containing components are only present in the lithiated state.[37]

Figure 3 shows similar results for the carbon coated electrode powder. As mentioned previously, 150 nm was known as the lower limit of crack formation in Si nanoparticles. However, cracks were observed in carbon-coated particles with a diameter lower than the previously mentioned limit (arrows in Figure 3a and g). We suggest that, during the lithiation-induced volume increase, the carbon coating applies some additional stress on the surface, causing the coating and particle to crack faster. The composition map in Figure 3b indicates that the initial oxide layer between the silicon and the carbon coating is kept intact during lithiation and still has the initial thickness of 4 nm. However, outside the carbon coating, Si^{4+} was also observed close to the crack in the coating. In these areas, electrolyte was able to react with silicon surface, resulting in the conversion of the native oxide layer into silicates. In the areas where the carbon coating shielded the silicon surface from the electrolyte, the native

oxide layer was kept intact. These observations clearly prove the creation of electrolyte-silicon interfaces at the level of the carbon crack. Consequently, the carbon coating is no longer fully protective even after only one electrochemical cycle. We managed to differentiate between the EELS signal of the carbon coating (Figure 4a) and another carbon source we observed at the outer surface of the particles (Figure 4d). The signal of the carbon coating is very similar to the signal of a graphite reference (Figure 4b) and clearly different from an amorphous carbon reference (Figure 4c). Consequently, the carbon coating has a graphite-like structure. The signature signal of the other carbon source at the outer surface of the particles is very similar to the signal of pure Li_2CO_3 (Figure 4e). The similarity of both EELS signals, suggests that the unknown signal originates from a compound (or family of compounds) very similar to Li_2CO_3. This suggests that the signal originates from alkyl carbonates in the SEI, formed by electrolyte decomposition. As a result, this fingerprint signal could be used in the future as a reference to map the presence of SEI in a carbon-based matrix, such as composite materials, making this a very powerful analysis tool. At the end of the first cycle, in the delithiated state (1.5 V), the initial oxide layer is still intact (Figure 3c and d). Furthermore, the morphology of the SEI layer is becoming more and more inhomogeneous. The thickness of the surface layer (SEI + coating) appeared to be larger in the lithiated than in delithiated state (24 ± 1 nm vs. 18 ± 1 nm), as was also the case with p-Si.

Figure 3e and f show the electrode material during the second cycle, in the lithiated state (0 V). The carbon coating shows more and more cracks and the morphology of the SEI becomes rougher. At the right side of Figure 3f, a separated piece of carbon coating with SEI at the surface was observed, indicating the process of degradation where the carbon coating detaches from the silicon surface. Also, similar to the case with p-Si, a lithium signal was observed at the surface of the particle. At the end of the second cycle, in the delithiated state (1.5 V), more cracks in coating and particles can be observed (Figure 3g). Figure 3h summarizes nicely the shielding effect of the carbon coating. In areas where the carbon

coating is still attached to the silicon surface, the native oxide layer is preserved. In areas where the coating was removed during the lithiation-induced volume changes, a lot of Si^{4+} was observed at the silicon surface, originating from silicates. A detached piece of the SEI can also be observed, highlighting the changes in morphology of the surface. In the delithiated state, no lithium signal was observed in the SEI layer.

2.1.2. Global study by EIS

p-Si and c-Si three electrode cells were electrochemically cycled over two charge-discharge cycles. At specific potentials, EIS spectra were recorded. The different features of a typical impedance spectrum are discussed in the experimental section. The evolution of the three most important parameters that were extracted from the recorded impedance spectra, $R_{SEI\ formation}$, R_{ct} and R_{film} is discussed below.

As illustrated in **Figure 5**, the impedance spectra present an inductive loop at low potentials, in both coated and uncoated samples. This phenomenon was first described by Radvanyi and Van Havenbergh *et al.*[19] The inductive loop is explained by a mechanism that states that both Li^+-ions and electrons are involved in a 2-step competitive reaction of the Volmer-Heyvrovsky-type, where lithium-insertion and SEI-formation are both interdependent. Via a set of analytical equations, the parameter $R_{SEI\ formation}$ is introduced in the equivalent circuit. $R_{SEI\ formation}$ (**Figure 6**) can be interpreted as the thermodynamical ease to form SEI. Since $R_{SEI\ formation}$ is related to the formation of SEI, it can be used as a tool to monitor at which potentials SEI is likely to be formed. To be clear: the couple $R_{SEI\ formation}//L_{SEI\ formation}$ in the equivalent circuit in Figure 5 solely describes the process of SEI-formation and not the irreversible capacity loss due to SEI-formation. The irreversible character of the SEI-formation is introduced by the $R_{film}//C_{film}$ circuit (SEI-deposit on the surface of the electrode) that highlights the fact that some compounds are kept on the electrode surface, whereas some are dissolved or removed from the surface.

In the beginning of the first lithiation of both the p-Si and c-Si electrode, $R_{SEI\ formation}$ has a high value until the potential reaches 0.15 V. A high value of $R_{SEI\ formation}$ means that SEI-formation on silicon surfaces is difficult in this potential region. However, this parameter does not give any information on other kinds of SEI-formation, such as the conversion of surface SiO_2 into silicates and SEI-formation of carbon surfaces. That is also the reason why the values of $R_{SEI\ formation}$ are lower in the case of c-Si, since most SEI is formed on carbon surface instead of silicon surface, because of a shielding effect of the carbon coating on the silicon surface.

As shown in Figure 1c in the experimental section, the first Li-insertion reaction of the pristine silicon material starts at 0.15 V. Below 0.15 V for both p-Si and c-Si, $R_{SEI\ formation}$ drops to a constant, low value. During the Li-insertion reaction, SEI-formation will become easier, until the lithiation ends at 0 V. The volume increase is linear to the Li-insertion, explaining the constant value of $R_{SEI\ formation}$. In the case of c-Si, cracks appear in the coating due to the volume increase and SEI is formed on the exposed silicon surface. During the delithiation and in the next cycle, the inductive loop was only observed in the potential region of the Li-insertion and Li-extraction process, with a decreasing value of $R_{SEI\ formation}$ with increasing potential. There are actually two possibilities for a low value of $R_{SEI\ formation}$: or SEI-formation is becoming easier (the inductive phenomenon is no more limiting and the inductive loop is becoming smaller) or the SEI-formation is stopping (the phenomenon is progressively disappearing and the inductive loop is becoming smaller). In this case, SEI-formation will stop for both electrode materials around 0.4 V in the delithiation (both cycle 1 and cycle 2) and start in the lithiation around 0.2 V (cycle 2).

The second parameter extracted from the impedance spectra is the charge transfer resistance (Figure 6). This parameter indicates the resistance that Li-ions encounter during the electron exchange when forming a Li-Si alloy. Intuitively, this resistance will be high at potentials where the Li-insertion process is not favored, as is the case above 0.15 V for both silicon

materials (pristine and coated) during the first lithiation (due to the amorphization process). The curves of R_{ct} present a sharp decrease at 0.15 V, indicating once more the start of the Li-insertion process at this potential. In addition to the similarities with p-Si, c-Si also has an additional decrease in R_{ct} around 0.8 V in the first cycle, which is linked to the Li-insertion reaction of the carbon coating.[23] Hence, the Li-insertion reaction will take place in a two-step process.

During the Li-insertion process in silicon, below 0.15 V, R_{ct} remains constant for both electrode materials. Ideally, the value should increase near 0 V; when fully lithiated, charge transfer will become more difficult, because the system will be almost saturated with lithium. Since the value of R_{ct} does not increase here, we can conclude that a fully lithiated state is not achieved. This is confirmed by the presence of a crystalline core in the TEM image in Figure 2b. The delithiation process is similar. Around 0.45 V, the curves for both electrode materials show an increase in charge transfer resistance, indicating that the Li-extraction process will become more difficult, since almost all Li-ions have been extracted from the silicon system. The increase in charge transfer resistance is less pronounced in the case of c-Si. The reason for this is the shielding effect of the carbon coating, which keeps the initial oxide layer intact. This SiO_2-layer is known to be insulating for Li-ions, acting as a trap for Li-ions during the Li-extraction process.[28] Since the charge transfer process is dependent upon the active surface area and especially the concentration gradient of the involved specie (Li^+), the Li-extraction process will be favored, resulting in a low value of R_{CT}. The second electrochemical cycle has similar evolutions for R_{ct} as the first. However, there is no sudden decrease during the lithiation as in the first cycle. R_{ct} decreases gradually from 1 V until 0.2 V. The difference is that after the first cycle, Si has become mainly amorphous, whereas it was crystalline before the first lithiation. Since the extra energy barrier for charge transfer caused by the amorphization process is not present in the second cycle, Li-insertion will already start at higher potentials. In the case of c-Si, the lithiation in the second electrochemical cycle starts

at the same low value of R_{ct} where the lithiation in the first cycle ended. Since the Li-extraction process was not completely finished, Li-insertion in the second cycle will start with less resistance.

Figure 6 shows the evolution of the surface film resistance (R_{film}). The term 'film' represents every layer at the surface of silicon (i.e. SEI layer, coating, etc.). Since the resistance is proportional to the thickness of the film (as well as proportional to the resistivity and inverse proportional to the active surface), this parameter is a useful tool to monitor the evolution of this surface film during cycling. Unfortunately, it is not possible to differentiate between the carbon coating and the SEI layer.[22, 23, 26] Both will contribute to one suppressed semi-circle in the impedance spectrum. The value for R_{film} is low during the first lithiation step in both electrode materials. In the case of p-Si, R_{film} increases slightly between 0.3 V and 0.2 V, followed by a sudden increase until a maximum value is reached at 0.15 V. The slight increase between 0.3 V and 0.2 V is attributed to the conversion of surface SiO_2 into lithium silicates, a process that typically takes place in this potential window.[30] This conversion results in a thicker surface film and hence a higher value for R_{film}. In the case of c-Si, R_{film} already starts increasing between 0.8 V and 0.2 V, the potential window where the SEI is formed on carbon surface. This illustrates that the SEI-formation here also follows a two-step process, with a formation on carbon surface between 0.8 V and 0.2 V and a formation on silicon at lower potentials. During the Li-insertion process, below 0.15 V, the value of R_{film} decreases slightly with both electrode materials. Bear in mind that the value is here proportional to the electrode surface, not the real active surface. If one would normalize the value with the active surface, thus correcting for the volume increase, the value of R_{film} would remain constant during the Li-insertion process. During the delithiation step in the first cycle, R_{film} shows a sudden decrease around 0.45 V, the potential where the Li-extraction process stops for both electrode materials (cfr. $R_{ct,}$). The dynamical behavior of the SEI at this point results in a decrease of R_{film}. The second electrochemical cycle is comparable to the first in

the case of p-Si, with the exception that in the lithiation step there is a more gradual increase in R_{film} starting from 0.6 V, as the Li-insertion reaction also starts at higher potentials compared to the first electrochemical cycle (cfr. R_{ct}). Since SEI-formation is not yet active at this potential (see $R_{SEI\ formation}$), the increase in R_{film} can be explained by the increase in surface area, due to the volume expansion and the dependence of R_{film} on this surface are. The delithiation step in the second cycle is very similar to the first cycle. In the case of c-Si, the second electrochemical cycle is somewhat different. The sharp increase in R_{film} during the lithiation appears only at very low potentials. This is also caused by the insulating effect of the unreacted oxide layer at the surface of silicon, due to the shielding effect of the carbon coating.

In conclusion, we have monitored that in the first lithiation, in the case of p-Si the surface SiO_2-layer is converted into lithium silicates between 0.3 V and 0.2 V. In the case of carbon-coated silicon, SEI-formation and Li-insertion in the coating take place between 0.8 V and 0.15 V. The alloying reaction between lithium and silicon and SEI-formation on silicon surface is active below 0.15 V. The dealloying reaction during the delithiation is active until 0.45 V. However, when a carbon coating is present, the native oxide layer at the surface of silicon, will block the Li-extraction process, resulting in very low values for R_{ct}.

2.2. Interface evolutions upon cycling

EIS results were also consistently acquired at the end of the lithiation (10 mV) and the end of the delithiation (1 V) during 30 electrochemical cycles**. Figure 7** compares the evolution of the three impedance parameters of p-Si with c-Si. In the case of p-Si, the evolution of $R_{SEI\ formation}$ has two drops: around cycle 4 and cycle 19. The first drop around cycle 4 can be attributed to a first pulverization of the electrode. Fresh silicon surface will be exposed to the electrolyte, resulting in the formation of new SEI and consequently a decrease in $R_{SEI\ formation}$. The pulverization of the electrode also translates into a decrease in R_{ct} (Figure 7c), because

the electrode reaction surface will increase.[41] Due to additional SEI-formation in the following cycles (cycle 5 until cycle 10), R_{ct} and $R_{SEI\ formation}$ will increase again. After cycle 10, both $R_{SEI\ formation}$ and R_{ct} decrease until cycle 18. Every electrochemical cycle, the electrode will pulverize more and new SEI will be formed. As described by *Radvanyi et al.*[29] and illustrated in Figure 2 and Figure 3, the interaction between the silicon particles and the SEI will no longer be purely core-shell. The SEI will start to detach from the surface and fill up bigger gaps in the electrode. In addition, the increased reaction surface will result in a decrease in R_{ct}. After a certain point, the 18th cycle in this case, the matrix will become more or less saturated with SEI.[29] Additional cycling will then not generate new SEI. Consequently, the inductive phenomenon attributed to the formation of SEI will go away and $R_{SEI\ formation}$ will become small or ultimately disappear. The evolution of R_{film} of p-Si is shown in Figure 7g. R_{film} increases gradually until cycle 18, after which the value decreases again. This first increase confirms that the SEI is fractionated upon cycling and that every cycle new SEI will be formed. The decrease after cycle 18 could be explained with electrode material that loses connectivity with the electrode due to volume changes and pulverization, thus no longer participating in the electrochemical reaction and contributing the averaged value of R_{film}.

In the case of c-Si, $R_{SEI\ formation}$ has a sudden decrease at cycle 2. The main SEI-formation on silicon surfaces will occur in the first cycle. In the consequent cycles, the inductive phenomenon will become small, since only new SEI on silicon surface will be formed when a crack appears in the carbon coating. The carbon coating will protect the silicon surface against most SEI-formation. Even though the carbon coating will crack, it will still cover most of the silicon surface. A small increase in $R_{SEI\ formation}$ can be observed around cycle 12, suggesting a small re-activation of the inductive phenomenon. At this point, the carbon coating will have degraded enough to make the surface behave more like the surface of p-Si. To confirm this,

an energy-dispersive X-ray (EDX) map was recorded after 30 electrochemical cycles (**Figure 8**a and b). The results for c-Si (Figure 8b) are very similar to p-Si (Figure 8a). It is no longer possible to distinguish a carbon coating at the surface of c-Si. For both the coated and uncoated electrode material, the silicon particles are completely fractionated after 30 cycles and covered with SEI. R_{ct} (Figure 7d) is even lower compared to p-Si. Besides from the first cycle where the value is higher, there is a gradual increase over cycling. This evolution of R_{ct} confirms that the carbon coating exhibits a shielding effect on the silicon particle. The Li-insulating native oxide layer is protected by the carbon coating and blocks the Li-insertion process of silicon. This theory is strengthened further with the evolution of R_{ct} in the delithiated state (1 V) (Figure 7f). The values here are low, whereas they are high and constant with p-Si (Figure 7e). As already described above, in a normal Li-extraction process, the charge transfer resistance is high in the delithiated state. In the case of c-Si however, the charge transfer resistance is low and gradually increases over cycling, since the shielding carbon coating is being destroyed during cycling and thus hindering the Li-extraction process less and less. The evolution of R_{ct} can therefore be used to monitor the degradation of the carbon coating. As the coating degrades, the charge transfer resistance will increase in both the lithiated and delithiated state. It is expected that Figure 7f will reach a plateau around 250 $\Omega.cm^2$, the value of p-Si, indicating the carbon coating has degraded completely and the charge transfer process behaves as a silicon-like system. R_{film} increases gradually (Figure 7h), indicating once more that the carbon coating is being degraded during cycling. The thickness of the SEI layer will hence increase accordingly. The loss of electrode material, as was the case for p-Si, is avoided here because the (fractured) carbon coating will retain the conductivity and connectivity of the electrode.

3. Conclusion

TEM observations confirm that the surface SiO_2-layer of the silicon nanoparticles is immediately converted into lithium silicate structures during the first lithiation. However, the application of a carbon coating effectively shields the native silicon surface from the electrolyte, avoiding a conversion into silicates. The unreacted SiO_2-layer appears to have an insulating effect for lithium, hindering the (de)alloying reaction of silicon. Despite the coating being 11 nm thick, the integrity is destroyed after just 2 cycles, causing a gradual conversion of SiO_2 into silicates and an exposure of the silicon surface to the electrolyte during further cycling. A thicker coating could be a valid approach but with consequences on the capacity. These observations were also confirmed by EIS measurements. The impedance parameters R_{ct} and R_{film} proved to be a simple tool to monitor the degradation of the carbon coating over cycling. Parameters $R_{SEI\ formation}$ and R_{ct} can be used to monitor the pulverization of the electrode. In this study, the 18^{th} electrochemical cycle showed to be a critical point for the pulverization of the electrode and the formation of SEI, which can easily be monitored via $R_{SEI\ formation}$ and R_{ct}. The main SEI-layer is formed during the first lithiation of the electrode, above 0.15 V, whereas during further electrochemical cycling, SEI is only formed on newly exposed silicon surfaces due to lithiation-induced volume changes, between 0.15 V and 0 V. In the case of carbon-coated silicon, a two-step process is active, where SEI-formation on the carbon surface takes place between 0.8 V and 0.15 V in the first lithiation. TEM observations also confirmed that the SEI is a dynamical layer, as the thickness is not constant during one electrochemical cycle. Furthermore, a trace of lithium ions was observed in the SEI only in lithiated state, whereas this was not the case for delithiated state. Finally, we managed to detect an EELS fingerprint for carbonate structures in the SEI layer, making it possible to map the SEI and differentiate it from a carbon matrix.

4. Experimental Section

Material characteristics: Two silicon nanopowders were used for this case study: a pristine, commercial nanopowder from Umicore (p-Si) and a carbon-coated variant (c-Si), synthesized by a thermal vapor deposition of toluene on the commercial nanopowder. Both powders have an average particle diameter of 50 nm. A TEM image of both initial materials is presented in Figure 1. p-Si has a specific surface area of 23 $m^2.g^{-1}$ and a native oxide layer thickness of 3 nm (Figure 1a). The crystallinity of the silicon particles is confirmed with the diffraction pattern as inset in Figure 1a. c-Si has a specific surface area of 20 $m^2.g^{-1}$, a native oxide layer of 4 nm and a carbon coating with a thickness of 11 nm. The thick carbon coating at the surface of c-Si can be observed in Figure 1b. The inset in the image shows that the carbon coating has a layered structure, with a graphite-like composition.

Electrode fabrication and battery assembly: Both silicon powders were used to make battery electrodes. For the electrochemical tests, an aqueous mixture of p-Si powder (80 wt %, Umicore), carbon black (12 wt %, Timcal C-NERGY SuperP) and CMC (8 wt %, Alfa Aesar) was used to produce a battery paste. In the case of c-Si, carbon black was left out of the mixture, while maintaining the ratio of active material and CMC. By using a doctor blade, the paste was coated onto a copper foil current collector at a thickness of 100 µm. After an initial drying at 70 °C, electrodes of 0.95 cm^2 were punched and dried overnight at 110 °C under vacuum, after which they were transferred into an argon-filled glove box. Here, 3-electrode Swagelok®-type cells were assembled. Metallic lithium was used as both counter and reference electrode. The electrodes were separated by glass fiber separators, soaked with electrolyte (1 M $LiPF_6$ in a 1:1 wt % mixture of ethylene carbonate (EC) and diethyl carbonate (DEC)).

For the TEM experiments, only silicon powder was used to make 2-electrode Swagelok®-type cells in a similar way as described above. In the case of p-Si, 13% of conducting carbon nanofibers (Showa Denko) were used to improve the conductivity.

Galvanostatic cycling was carried out with a Biologic® VMP3 machine.

Electrochemical fingerprints: As can be seen from Figure 1c, both silicon powders have a similar galvanostatic behavior in the first cycle of lithiation/delithiation and feature an amorphization plateau during lithiation around 50 mV. During delithiation there is a plateau in the galvanostatic curve at 420 mV. It is clear that p-Si (3850 $mAh.g^{-1}$) reaches a higher capacity than c-Si (2600 $mAh.g^{-1}$), because c-Si consists of almost 30% of carbon material, contributing to a lower theoretical capacity (3304 $mAh.g^{-1}$ for p-Si compared to 2340 $mAh.g^{-1}$ for c-Si). Note that both measured capacities exceed the theoretical value, indicating irreversible capacity loss due to SEI formation. Furthermore, p-Si has a much higher irreversible capacity loss in the first cycle compared to c-Si (442 $mAh.g^{-1}$ and 298 $mAh.g^{-1}$ resp.). The carbon coating provides a better protection of the silicon surface, changing the surface chemistry and resulting in less and/or different SEI formation. In addition, the good conductivity of the carbon coating will also improve the electrical integrity of the electrode.

Figure 5 compares the impedance spectra of both electrode materials at 0.2 V in delithiated state of the first electrochemical cycle. Several regions in the impedance spectra can be differentiated: a semi-circle in the high-frequency region (~30 kHz) originating from a film at the surface (SEI, SEI + coating, …), a mid-frequency semi-circle (100-2000 Hz) characterizing the charge transfer at the silicon surface and a low-frequency region associated with diffusion of Li^+ into silicon bulk. An equivalent electrical circuit (inset in Figure 5) was used to fit the recorded impedance spectra, by calculating values for the different parameters in the equivalent circuit.

TEM measurements: TEM measurements were performed at several stages during lithiation and delithiation. 2-Electrode batteries were cycled at a C-rate of C/100, after which they were transferred to an argon-filled glove box and opened. The reacted electrode powder was soaked for 1 minute in pure DEC to wash off remaining Li-salts. Afterwards, the powder was dispersed in DEC and dropped onto a holey carbon film, coated on a copper mesh TEM grid.

This grid was mounted onto a specialized Gatan TEM holder, to transfer the sample from glove box to microscope without contact to air.

All battery samples were investigated on an FEI TITAN 80-300 "cubed" microscope equipped with an aberration-corrector for the probe forming lens and operated at 120 kV acceleration voltage. Electron energy-loss spectroscopy (EELS) measurements were performed in scanning transmission electron microscopy (STEM) mode. Typical experimental settings used were; convergence angle α of 22 mrad, EELS collection angle β of 61 mrad, spectra acquired at an energy dispersion of 0.5 eV/pixel. To generate the chemical maps, the EELS spectra in the acquired "spectrum image" datacubes were fitted in the EELSModel[32] software package using a power-law background AE^{-r} combined with reference spectra (for Si^0, Si^{4+}, the carbon coating and the carbonaceous SEI). The intensities of the reference components as well as the power-law background were fitted to the acquired spectra, and the signal intensities were plotted to generate the component maps. The model was fitted using a Levenberg-Marquardt method for Poisson statistics. Energy-dispersive X-ray (EDX) measurements were performed with a Tecnai Osiris microscope, equipped with a Super-X detector and operated at 200 kV acceleration voltage.

EIS measurements: The 3-electrode batteries for EIS measurements were cycled at a C-rate of C/50, using a Biologic® VMP3 machine. All EIS measurements were performed after a CV-step at the desired potential for 2 hours, after which the deviation of the current was smaller than 5 $\mu A.h^{-1}$. The perturbation amplitude was 5 mV and the frequency was scanned in a range from 100 kHz to 100 mHz. Zview software was used to fit the acquired impedance spectra.

Acknowledgements
K. Van Havenbergh gratefully acknowledges IWT Flanders for the financial support. Prof. Sylvain Franger is also gratefully acknowledged for the fruitful discussions on EIS modelling.

Received: ((will be filled in by the editorial staff))
Revised: ((will be filled in by the editorial staff))
Published online: ((will be filled in by the editorial staff))

[1] M. Armand, J. M. Tarascon, Nature 2008, 451, 652.
[2] J. M. Tarascon, M. Armand, Nature 2001, 414, 359.
[3] R. Teki, M. K. Datta, R. Krishnan, T. C. Parker, T.-M. Lu, P. N. Kumta, N. Koratkar, Small 2009, 5, 2236.
[4] K. Mizushima, P. C. Jones, P. J. Wiseman, J. B. Goodenough, Materials Research Bulletin 1980, 15, 783; H. Yu, H. Kim, Y. Wang, P. He, D. Asakura, Y. Nakamura, H. Zhou, Physical Chemistry Chemical Physics 2012, 14, 6584.
[5] J. S. Bridel, T. Azais, M. Morcrette, J. M. Tarascon, D. Larcher, Journal of the Electrochemical Society 2011, 158, A750.
[6] A. N. Dey, Journal of the Electrochemical Society 1971, 118, 1547.
[7] M. N. Obrovac, L. Christensen, Electrochemical and Solid State Letters 2004, 7, A93; L. Y. Beaulieu, T. D. Hatchard, A. Bonakdarpour, M. D. Fleischauer, J. R. Dahn, Journal of the Electrochemical Society 2003, 150, A1457.
[8] M. K. Y. Chan, C. Wolverton, J. P. Greeley, Journal of the American Chemical Society 2012, 134, 14362.
[9] W.-J. Zhang, Journal of Power Sources 2011, 196, 13.
[10] X. H. Liu, L. Zhong, S. Huang, S. X. Mao, T. Zhu, J. Y. Huang, Acs Nano 2012, 6, 1522.
[11] Y. C. Yen, S. C. Chao, H. C. Wu, N. L. Wu, Journal of the Electrochemical Society 2009, 156, A95.
[12] B. Philippe, R. Dedryvere, J. Allouche, F. Lindgren, M. Gorgoi, H. Rensmo, D. Gonbeau, K. Edstrom, Chemistry of Materials 2012, 24, 1107.
[13] X. H. Liu, Y. Liu, A. Kushima, S. Zhang, T. Zhu, J. Li, J. Y. Huang, Advanced Energy Materials 2012, 2, 722.
[14] C. K. Chan, R. Ruffo, S. S. Hong, R. A. Huggins, Y. Cui, Journal of Power Sources 2009, 189, 34; M. T. McDowell, S. W. Lee, J. T. Harris, B. A. Korgel, C. M. Wang, W. D. Nix, Y. Cui, Nano Letters 2013, 13, 758; C. K. Chan, R. Ruffo, S. S. Hong, Y. Cui, Journal of Power Sources 2009, 189, 1132.
[15] H. Wu, Y. Cui, Nano Today 2012, 7, 414; J. R. Szczech, S. Jin, Energy & Environmental Science 2011, 4, 56; H. J. Gao, B. H. Ji, I. L. Jager, E. Arzt, P. Fratzl, Proceedings of the National Academy of Sciences of the United States of America 2003, 100, 5597.
[16] H. Nara, T. Yokoshima, T. Momma, T. Osaka, Energy & Environmental Science 2012, 5, 6500; M. Schmuck, A. Balducci, B. Rupp, W. Kern, S. Passerini, M. Winter, Journal of Solid State Electrochemistry 2010, 14, 2203.
[17] I. Kovalenko, B. Zdyrko, A. Magasinski, B. Hertzberg, Z. Milicev, R. Burtovyy, I. Luzinov, G. Yushin, Science 2011, 334, 75; C. Erk, T. Brezesinski, H. Sommer, R. Schneider, J. Janek, Acs Applied Materials & Interfaces 2013, 5, 7299.
[18] J. S. Bridel, T. Azais, M. Morcrette, J. M. Tarascon, D. Larcher, Chemistry of Materials 2010, 22, 1229; N. S. Hochgatterer, M. R. Schweiger, S. Koller, P. R. Raimann, T. Woehrle, C. Wurm, M. Winter, Electrochemical and Solid State Letters 2008, 11, A76.
[19] E. Radvanyi, K. Van Havenbergh, W. Porcher, S. Jouanneau, J.-S. Bridel, S. Put, S. Franger, Electrochimica Acta 2014, 137, 751.
[20] N. S. Choi, K. H. Yew, K. Y. Lee, M. Sung, H. Kim, S. S. Kim, Journal of Power Sources 2006, 161, 1254; M. Itagaki, S. Yotsuda, N. Kobari, K. Watanabe, S. Kinoshita, M. Ue, Electrochimica Acta 2006, 51, 1629; L. Martin, H. Martinez, M. Ulldemolins, B. Pecquenard, F. Le Cras, Solid State Ionics 2012, 215, 36.
[21] L. Su, Y. Jing, Z. Zhou, Nanoscale 2011, 3, 3967; L. Su, Z. Zhou, M. Ren, Chemical Communications 2010, 46, 2590.

[22] J. Guo, A. Sun, X. Chen, C. Wang, A. Manivannan, Electrochimica Acta 2011, 56, 3981.
[23] W. R. Liu, J. H. Wang, H. C. Wu, D. T. Shieh, M. H. Yang, N. L. Wu, Journal of the Electrochemical Society 2005, 152, A1719.
[24] J. K. Lee, W. Y. Yoon, B. K. Kim, Journal of the Electrochemical Society 2012, 159, A1844.
[25] X. W. Zhang, P. K. Patil, C. S. Wang, A. J. Appleby, F. E. Little, D. L. Cocke, Journal of Power Sources 2004, 125, 206.
[26] P. J. Zuo, G. P. Yin, Y. L. Ma, Electrochimica Acta 2007, 52, 4878.
[27] N. Dimov, K. Fukuda, T. Umeno, S. Kugino, M. Yoshio, Journal of Power Sources 2003, 114, 88; N. Dimov, S. Kugino, M. Yoshio, Electrochimica Acta 2003, 48, 1579.
[28] S. Xun, X. Song, L. Wang, M. E. Grass, Z. Liu, V. S. Battaglia, G. Liu, Journal of the Electrochemical Society 2011, 158, A1260.
[29] E. Radvanyi, W. Porcher, E. De Vito, A. Montani, S. Franger, S. J. S. Larbi, Physical Chemistry Chemical Physics 2014, 16, 17142.
[30] T. L. Kulova, A. M. Skundin, Y. V. Pleskov, E. I. Terukov, O. I. Kon'kov, Journal of Electroanalytical Chemistry 2007, 600, 217.
[31] E. Pollak, G. Salitra, V. Baranchugov, D. Aurbach, Journal of Physical Chemistry C 2007, 111, 11437; R. Ruffo, S. S. Hong, C. K. Chan, R. A. Huggins, Y. Cui, Journal of Physical Chemistry C 2009, 113, 11390; H. Schranzhofer, J. Bugajski, H. J. Santner, C. Korepp, K. C. Moller, J. O. Besenhard, M. Winter, W. Sitte, Journal of Power Sources 2006, 153, 391; Q. C. Zhuang, Z. F. Chen, Q. F. Dong, Y. X. Jiang, L. Huang, S. G. Sun, Chinese Science Bulletin 2006, 51, 1055; S. S. Zhang, K. Xu, T. R. Jow, Electrochimica Acta 2004, 49, 1057; S. S. Zhang, M. S. Ding, K. Xu, J. Allen, T. R. Jow, Electrochemical and Solid State Letters 2001, 4, A206; S. S. Zhang, K. Xu, T. R. Jow, Electrochimica Acta 2006, 51, 1636.
[32] www.eelsmodel.ua.ac.be.
[33] M. Schade, N. Geyer, B. Fuhrmann, F. Heyroth, H. S. Leipner, Applied Physics a-Materials Science & Processing 2009, 95, 325.
[34] P. Limthongkul, Y. I. Jang, N. J. Dudney, Y. M. Chiang, Journal of Power Sources 2003, 119, 604.
[35] X. H. Liu, H. Zheng, L. Zhong, S. Huan, K. Karki, L. Q. Zhang, Y. Liu, A. Kushima, W. T. Liang, J. W. Wang, J.-H. Cho, E. Epstein, S. A. Dayeh, S. T. Picraux, T. Zhu, J. Li, J. P. Sullivan, J. Cumings, C. Wang, S. X. Mao, Z. Z. Ye, S. Zhang, J. Y. Huang, Nano Letters 2011, 11, 3312.
[36] B. Philippe, R. Dedryvere, M. Gorgoi, H. Rensmo, D. Gonbeau, K. Edstrom, Journal of the American Chemical Society 2013, 135, 9829.
[37] B. Philippe, R. Dedryvere, M. Gorgoi, H. Rensmo, D. Gonbeau, K. Edstrom, Chemistry of Materials 2013, 25, 394.
[38] H. Bryngelsson, M. Stjerndahl, T. Gustafsson, K. Edstrom, Journal of Power Sources 2007, 174, 970.
[39] P. B. Balbuena, Y. Wang, Imperial College Press: London, UK 2004; C. Pereira-Nabais, J. Swiatowska, A. Chagnes, A. Gohier, S. Zanna, A. Seyeux, P. Tran-Van, C.-S. Cojocaru, M. Cassir, P. Marcus, Journal of Physical Chemistry C 2014, 118, 2919.
[40] C. Pereira-Nabais, J. Swiatowska, A. Chagnes, F. Ozanam, A. Gohier, P. Tran-Van, C.-S. Cojocaru, M. Cassir, P. Marcus, Applied Surface Science 2013, 266, 5.
[41] R. Ahmed, K. Reifsnider, International Journal of Electrochemical Science 2011, 6, 1159.

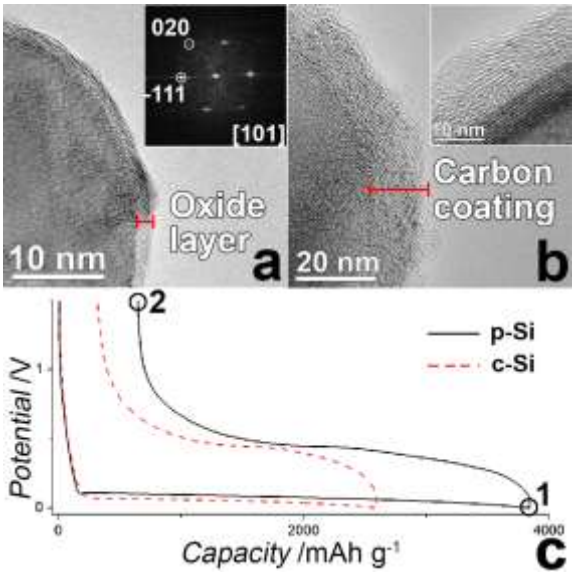

Figure 1. (a, b) TEM images of (a) p-Si with a clear indication of the amorphous oxide layer at the surface and the crystallinity of the Si core (FFT in inset) and (b) c-Si with the layered, graphitic carbon coating (higher magnification of the carbon coating in inset).
(c) galvanostatic curve of the first complete electrochemical cycle of both p-Si and c-Si. The electrodes were cycled between 0.01 V and 1.5 V. Numbers 1 and 2 indicate the stages of TEM measurement in the first cycle. The TEM measurements in the second cycle were performed at similar potentials.

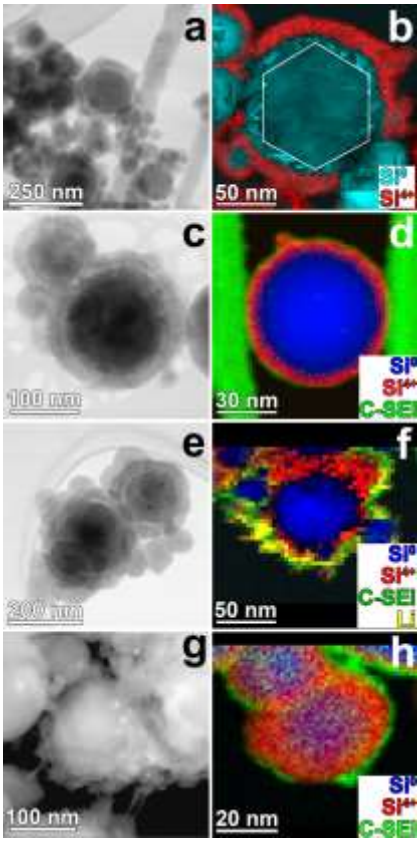

Figure 2. TEM images (a, c, e, g) and chemical maps (b, d, f, h) of p-Si particles at different states in the (de)lithiation process. (a, b) lithiated state (0 V) in the first cycle; (c, d) delithiated state (1.5 V) in the first cycle; (e, f) lithiated state (0 V) in the second cycle; (g, h) delithiated state (1.5 V) in the second cycle.

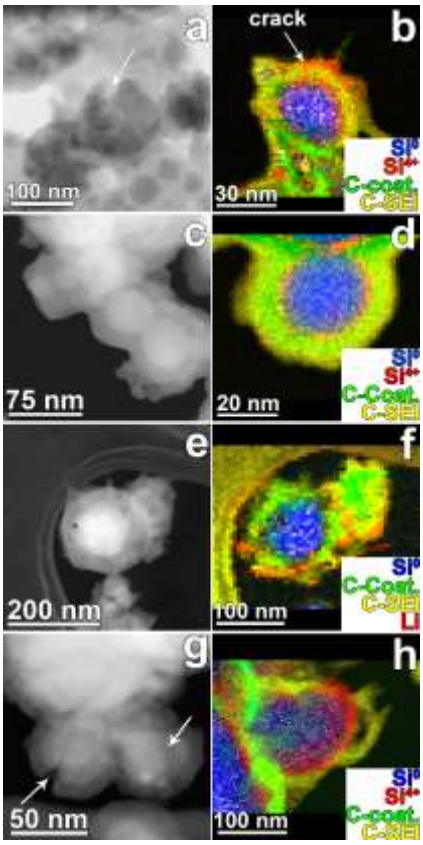

Figure 3. TEM images (a, c, e, g) and chemical maps (b, d, f, h) of c-Si particles at different states in the (de)lithiation process. (a, b) lithiated state (0 V) in the first cycle; (c, d) delithiated state (1.5 V) in the first cycle; (e, f) lithiated state (0 V) in the second cycle; (g, h) delithiated state (1.5 V) in the second cycle.

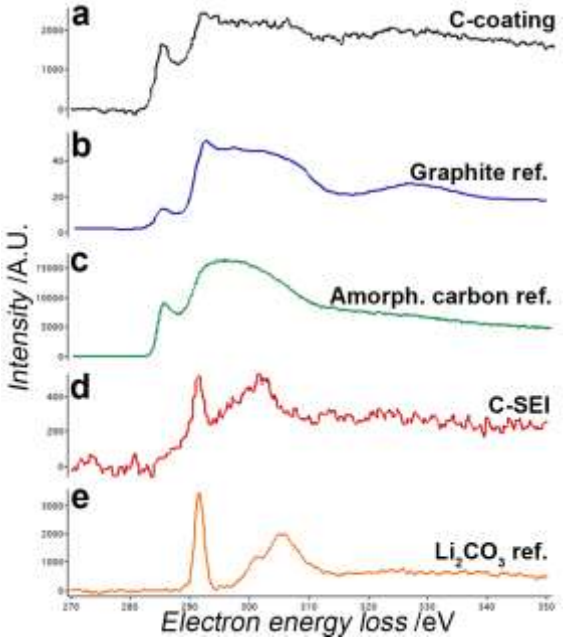

Figure 4. EELS fingerprint spectrum of (a) the carbon coating of c-Si, (b) a graphite reference, (c) an amorphous carbon reference, (d) the carbonaceous SEI and (e) a pure Li_2CO_3 reference.

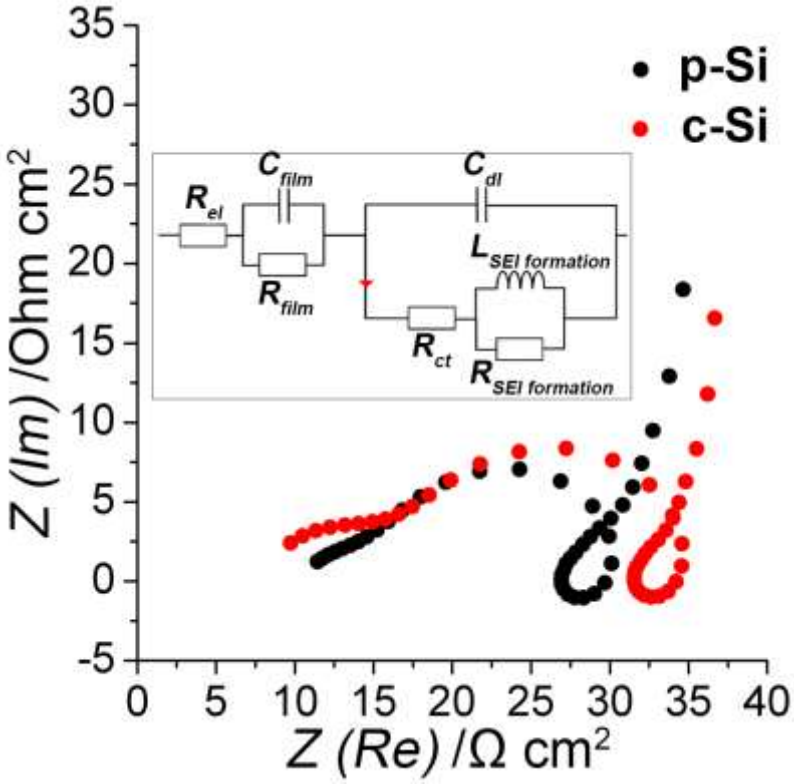

Figure 5. Typical impedance spectrum for p-Si and c-Si, recorded at 0.2 V during delithiation in the first electrochemical cycle. Inset: equivalent electrical circuit used for spectra fitting.

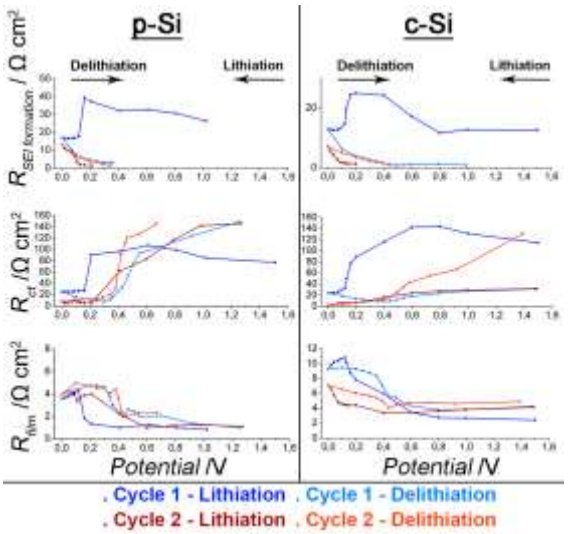

Figure 6. Evolution of $R_{SEI\ formation}$, R_{ct} and R_{film} obtained for the EIS spectra of p-Si and c-Si during the first two electrochemical cycles.

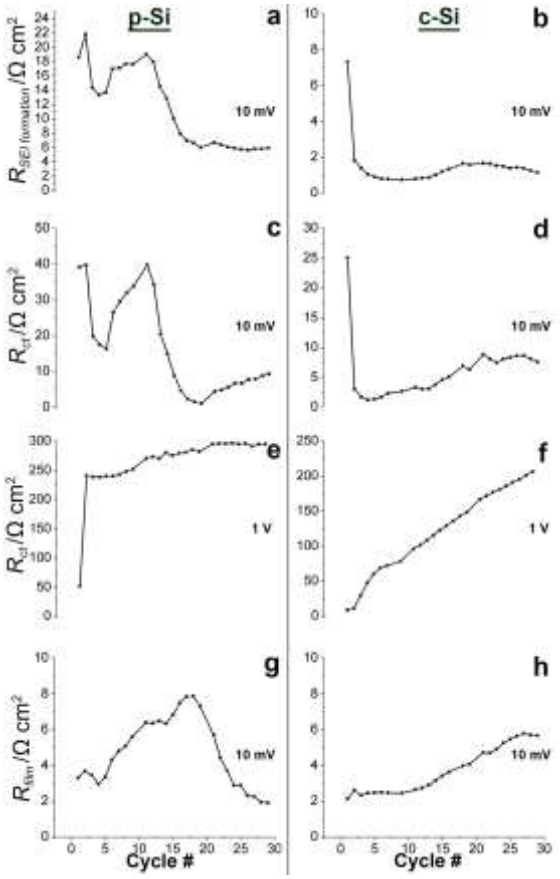

Figure 7. Evolution of the parameters obtained for the EIS spectra during the first 30 electrochemical cycles of p-Si (a, c, e, g) and c-Si (b, d, f, h). (a, b) $R_{SEI\ formation}$ (10 mV); (c, d) R_{ct} (10 mV), (e, f) R_{ct} (1 V) and (g, h) R_{film} (10 mV).

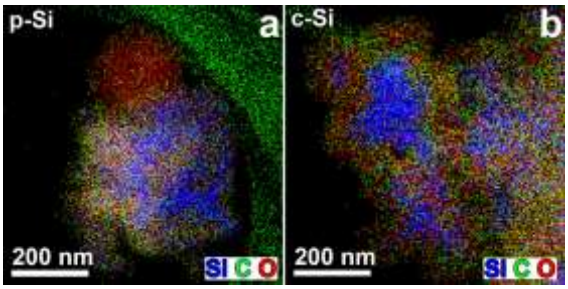

Figure 8. EDX map of (a) p-Si and (b) c-Si at the end of 30 electrochemical cycles.

The impact of a thin carbon coating at the surface of Si nanoparticles on the formation and evolution of the SEI is monitored during the first electrochemical cycles by TEM, EELS and impedance spectroscopy. TEM measurements demonstrate a shielding effect of the carbon coating on the native SiO_2-layer, while EIS measurements enable a fast monitoring of the SEI-formation.

Keyword: Li-ion batteries, coated silicon nanoparticles, SEI, impedance spectroscopy, TEM

K. Van Havenbergh, S. Turner, K. Driesen, J.-S. Bridel*, G. Van Tendeloo

Monitoring of the SEI-Evolution of Uncoated and Carbon-Coated Si Nanoparticles by Transmission Electron Microscopy and Electrochemical Impedance Spectroscopy